Macrophage-derived fusogenic nanovesicle for detection of atherosclerotic plaque progression

Lee, Ji-Youn

Department of Medical Science

Graduate School

Yonsei University

Macrophage-derived fusogenic nanovesicle for detection of atherosclerotic plaque progression

Advisor Sung, Hak Joon

A Master's Thesis Submitted
to the Department of Medical Science
and the Committee on Graduate School
of Yonsei University in Partial Fulfillment of the
Requirements for the Degree of
Master of Medical Engineering

Lee, Ji-Youn

July 2025

Macrophage-derived fusogenic nanovesicle for detection of atherosclerotic plaque progression

This certifies that the Master's Thesis of Ji-Youn Lee is approved

Thesis Supervisor Sung, Hak Joon

Thesis Committee Member Gee, Heon Yung

Thesis Committee Member Jin, Yoon Hee

The Graduate School
Yonsei University

July 2025

ACKNOWLEDGEMENTS

어느새 석사 학위과정을 마치고 학위논문을 제출하게 되었습니다. 모두 2년간 많은 분들의 응원과 도움이 있었기에 가능한 일이었습니다. 이렇게 짧게라도 글로 감사의 말씀을 전합니다.

우선, 부족한 저를 많은 기회와 지원을 아끼지 않고 때론 꾸짖으면서도 올바른 방향으로 나아갈 수 있도록 지도해주신 성학준 교수님께 깊은 감사드립니다.

또한 먼저 바쁘신 와중에도 함께 연구를 진행하면서 학문적으로 많은 조언을 아끼지 않으신 정세용 박사님과 하현수 박사님께 감사드립니다. 갈피를 못 잡는 저에게 항상 든든한 버팀목이 되어주신 백세움 박사님과 언제나 학생들을 챙겨 주시던 조성우 박사님께도 감사드립니다.

함께 밤낮으로 실험 고민을 해가며 가족처럼 의지할 수 있었던 찬식쌤, 주은이에게도 감사합니다. 모두 노력한 그 이상으로 훌륭한 연구자가 될 것이라 믿습니다. 항상 웃게 해준 현재오빠, 석준쌤, 실험실을 떠난 후에도 응원을 아까지 않은 혜원언니, 수지언니, 시영언니에게도 감사합니다. 석사과정 동안 함께한 모든 재생의공학교실 식구들에게 진심으로 감사드립니다.

그리고 2년간 달려오며 지쳤을 때 재충전시켜주며 일으켜 준 고마운 친구들 다현이, 승은이, 세연이, 나현이, ISED 동기들, ASFM 친구들, 클로버 동생들, 모두 저에게 큰 힘이 되었습니다. 고맙습니다.

마지막으로, 해외를 오가며 길었던 배움의 시간동안 지원을

아끼지 않으면서 묵묵히 응원해준 사랑하는 우리 엄마, 아빠에게 온 마음을 다해 감사드립니다. 이제는 제가 보답하기 위해 더 잘 하도록 하겠습니다. 그리고 언제나 동생 고민을 들어주고 도와준 다정한 우리 오빠에게도 고마움을 전합니다.

TABLE OF CONTENTS

LIST OF FIGURES

LIST OF TABLES

ABSTRACT

Macrophage-derived fusogenic nanovesicle for detection of atherosclerotic plaque progression

Macrophages have an inherent ability to fuse together and form multinucleated giant cells under certain stimuli. During this process, macrophages become fusogenic and upregulate specific fusion-mediating surface proteins that facilitate homotypic fusion. Cell-derived vesicles can be produced with cell membranes at specific time points of cell physiology, resulting in vesicles that reflect the physiological state of the cell. Here, we propose a novel macrophage-targeted drug delivery system using fusogenic macrophage-derived nanovesicles (F-MNVs). F-MNVs retain fusion mediators in the fusogenic state, allowing them to serve as naturally occurring macrophage targeting moieties. These F-MNVs exhibit selective uptake by macrophages among mixed cell populations. In addition, unlike conventional nanoparticle uptake, F-MNVs fuse with macrophage membranes and deliver their cargo directly into the cytosol, bypassing endosomal entrapment and lysosomal degradation. In a rabbit model of atherosclerosis, injected F-MNVs efficiently targeted macrophage-rich plaques, confirming their potential as a precise, biologically derived platform for drug delivery in inflammatory diseases.

Key words : cell-derived nanovesicle, macrophage fusion, drug delivery system, atherosclerosis

1. Introduction

Atherosclerosis is a key underlying condition in cardiovascular disease and one of the primary causes of mortality worldwide. It is a chronic inflammatory disease marked by the buildup of lipids and inflammation resulting in plaque formation along the inner wall of the arteries. Initiated by endothelial activation and followed by the progression of a non-resolving cascade of events, the formation of atherosclerotic plaques leads to cardiovascular complications. While most plaques remain clinically silent, some lesions become prone to rupture, leading to acute cardiovascular events. Current anti-atherosclerotic therapies focus on two main approaches: pharmaceutical treatments to reduce plaque formation and stabilize existing plaques, and surgical interventions to mechanically open narrowed arteries and remove plaque. However, current modalities are inadequate for predicting high-risk plaques that are prone to acute events.[1-3,6]

Macrophages fulfill a multitude of pivotal roles in the immune system, including the engulfment and digestion of foreign matter for host defense and tissue repair. Given its functional diversity, macrophage dysregulation is implicated in major immune diseases such as tumor and atherosclerosis. Macrophages are the predominant immune cells in atherosclerotic plaques and contribute to plaque instability by releasing inflammatory precursors, including proteases, reactive oxygen species, and immune mediators. Therefore, macrophages are emerging as a potential target for the diagnosis of vulnerable plaques.[3]

Nanotherapeutics refer to the delivery of nanoscale therapeutic agents to specific targeted regions within the body. The field has recently garnered interest due to their small diameter, which enables penetration of physiological barriers, stability in circulation, and engineering for specific cell recognition.[5] Nanoparticles are typically derived from synthetic materials including liposomes, metals, and polymers. These particles are often fabricated to possess targeting agents along the surface for successful drug delivery. However, it is a challenging task for effective and specific delivery of nano-drug carriers as foreign particles within circulation are recognized for excretion.

Cell-derived nanovesicles are appealing due to its ability to evade immune surveillance, and its homing ability to its cell of origin. These exosome-like particles are capable of large-scale production, which surpasses the constraints of naturally secreting exosomes because of its large-scale production capability. Cells are mechanically disrupted to form nanovesicles of which its surface retains the characteristics of the cell membrane upon the state of extrusion, and its void center can be manipulated to deliver therapeutic agents. Macrophage derived nanovesicles (MNV) therefore can target macrophages even among mixed cell populations. Their cell-like membrane cloak allows escape immune recognition. Moreover, macrophages possess an inherent capacity to fuse into multinucleated giant cells. Its homotypic fusion can be induced through cytokines, particularly interleukin-4 (IL-4).[4] Fusion-competent macrophages express additional naturally induced fusion mediators without addition of synthetic materials for enhanced homotypic adhesion to macrophages.

Hence, it is necessary to develop a highly specific and effective macrophage targeting agent. Fusion-competent macrophage derived nanovesicles (F-MNV) with organic surface molecules that can fuse specifically to macrophages can serve as a promising targeting modality for the unmet need of atherosclerotic plaque diagnosis methods.

Targeted drug delivery is a system of direct targeting of the drug moiety to its target site in the body in order to overcome the aspecific toxic effect of conventional drug delivery, thereby reducing the amount of drug required for therapeutic efficacy.[7] However, drug delivery strategies face significant challenges, particularly when it comes to targeting specific cells or tissues upon blood circulation. Nanoparticles are subject to biological clearance by opsonization-mediated removal of nanoparticles by immune cells and filtration by organs with fenestrated vasculature.[9] Surface-engineered molecules are developed to enhance blood circulation time and evade immune clearance such as modifying nanoparticles to express targeting ligands to specifically accumulate into the target area for cellular uptake.

Unfortunately, even when nanocarriers are engulfed by the target cell, only a few percent can reach the cytosol after endosomal/lysosomal entrapment.[10] Therefore, there is ongoing reserach for ways to overcome endosomal delivery. One promising mechanism is the direct fusion of carriers with the cell membrane, which could directly deliver the encapsulated cargo into target cell cytoplasm.[8] Macrophages possess the ability to fuse into multinuclear giant cells upon intracellular fusion inducing factor such as the cytokine IL-4. Upon those stimuli, macrophages become fusion-competent, leading to macrophage fusion. Induction of a fusion-competent status is known to involve several fusion mediators. Bone marrow monocyte derived macrophages (BMDM) are known to have the capacity to induce giant cell formation *in vitro* and *in vivo* under IL-4 stimulation. Fusion-competent macrophages express molecular mediators on the surface of their membranes that are crucial for macrophage-macrophage recognition. Mechanical disruption and extrusion of macrophage membranes at this status through nanosized pores will result in fusion-competent macrophage nanovesicles which retain the macrophage homotypic fusion ability through molecular adhesion factors.

Targeted therapies for atherosclerosis using nanoparticles are particularly challenging because the plaque site of the atherosclerotic area is small and the blood flow/pressure in the vessel is high, making it difficult for nanoparticles to remain in the lesion sites in large quantities, thus posing a hurdle for clinical use.[11] Moreover, atherosclerosis is an irreversible cascade of events leading to atheroma plaque formation. Drug delivery to already existing plaques are incapable of treating the disease. Thus, targeting agents must be developed for early diagnosis of rupture-prone plaques. Atheroma development initiates upon vascular endothelium dysfunction and monocyte recruitment. The endothelial monolayer becomes activated through certain stimuli and become leaky and induce selective monocyte recruitment into the intima to be differentiated into macrophages. These two primary characteristics of plaque development enable MNVs to effectively target early atherosclerotic lesions. First, MNVs can passively target the damaged endothelial layer through enhanced permeability and retention (EPR) effect.[12] Endothelial cell dysfunction increases the permeability of the endothelial layer. Nanoagents can penetrate the incomplete endothelium and

accumulate at the target site through its characteristic size. Secondly, MNVs can actively target plaques because of their surface macrophage-targeting ligands.

Here, we create MNV and F-MNV through extrusion of macrophage membranes and utilize their surface molecules for homotypic macrophage specific uptake for the early diagnosis of vulnerable plaques. MNVs are generated, and its targeting ability are confirmed through *in vitro* plaque mimetic environment and *in vivo* atherosclerotic plaque carotid artery model.

2. Materials and Methods

2.1. Fusogenic macrophage differentiation and culture

All animal procedures were approved by the Institutional Animal Care and Use Committee (IACUC) of Yonsei University College of Medicine (Approval No. #2022-0208 for mouse studies and #2023-0101 for rabbit studies). Fusogenic macrophages were obtained from the bone marrow of 6-week-old male C57BL/6 wild-type mice (Orient Bio, Seoul, Republic of Korea) after euthanasia by CO_2 inhalation. The femurs and tibias were dissected, and the epiphyseal ends near the knees were cut to access the metaphysis.[13] For bone marrow collection, a sterile 0.7 mL microcentrifuge tube (punctured at the base with a 20-gauge needle) was nested inside a 1.7 mL tube. The bones were placed vertically with the cut ends facing down and centrifuged at 10,000 × g for 15 seconds to extract the bone marrow. The resulting cell pellet was treated with 1X RBC lysis buffer (420302, BioLegend, San Diego, CA, USA) prepared in distilled water per mouse and incubated for 3 minutes with gentle agitation every 30 seconds. The cells were then centrifuged at 700 × g for 3 minutes, washed with complete DMEM, and filtered through a 70 μm sieve to remove clumps and debris. The cell suspension was adjusted to 1×10^6 cells/mL with a mixture of complete DMEM and macrophage differentiation medium in an 8:2 ratio and seeded onto nonadherent Petri dishes. The macrophage differentiation medium was prepared as 2-week conditioned medium from 1×10^5 L-929 mouse fibroblasts cultured in a 175 cm^2 flask, providing macrophage colony stimulating factor (M-CSF) essential for differentiation. Cells were incubated for 6 days, with fresh differentiation medium added on day 3. On day 6, to induce fusogenic activation, the medium was replaced with complete DMEM supplemented with 100 ng/mL murine IL-4 (214-14-100, PeproTech Inc., Rocky Hill, NJ, USA) and 10 ng/mL M-CSF (315-02, PeproTech). Cells were collected from the petri dish by gentle PBS washing twice.

2.2. Production of macrophage nanovesicles(MNV) and liposomes

2.2.1. MNV and Fusogenic-MNV(F-MNV) Production

Macrophages were cultured in differentiation media and detached from petri dishes by gentle pipetting with PBS at specific differentiation time points: immature macrophages were collected on day 3, mature macrophages on day 6, and fusogenic macrophages 3 days after activation of mature macrophages. For nanovesicle production, cells were centrifuged at 700 × g and resuspended in hypotonic cell lysis buffer at a density of 1×10^8 cells/mL. The buffer contained 1X protease inhibitor cocktail (78440, Thermofisher) and 1.5 mM $MgCl_2$ (M1028, Sigma-Aldrich, St. Louis, MO, USA). The suspension was incubated at 4 °C for 20 minutes. Cell lysis was achieved through

mechanical disruption by passing the suspension 80 times through a Mini-Extruder (610000, Avanti Polar Lipids Inc., Alabaster, AL, USA). Unbroken cells and debris were pelleted by centrifugation at 700 × g for 12 minutes. The supernatant was harvested and centrifuged at 14,000 × g for 40 minutes to isolate nanovesicles. The pellet was resuspended in PBS and extruded 13 times through a 0.4 μm membrane filter (800282, Cytiva, Marlborough, MA, USA) sandwiched between two drain discs (PETEDD9025, Sterlitech Corporation, Auburn, WA, USA). Gold nanovesicles were produced by resuspending the pellet in 1 mL of 30 nm gold nanoparticle suspension (753629, Sigma-Aldrich) prior to extrusion. Succesful coating of gold nanovesicles can be observed by their retainment of the characteristic cherry-red color of gold nanoparticle solution. Nanovesicles were quantified using the BCA protein assay kit (23227, Thermofisher), measuring surface protein amounts to determine NV concentration. For 70 kDa FTIC-dextran (46945, Sigma-Aldrich) loaded Macrophage NV(MNV) and fusogenic MNV (F-MNV), dextran treated medium was treated overnight to macrophages before cell lysis. Nanovesicles were stored in pellets within a deep freezer (- 80°C) for storage up to 1 month.

2.2.2. Liposome production

Liposomes were manufactured using the rapid ethanol injection method.[14] Phospholipids dissolved in ethanol were rapidly injected into PBS. As ethanol diffused, phospholipids self-assembled into bilayer structures to minimize contact with the aqueous phase. The lipid mixture was prepared by combining dipalmitoyl phosphatidylcholine (850355P, Sigma-Aldrich), cholesterol (C8667, Sigma-Aldrich), and 1,2-distearoyl-sn-glycero-3-phosphoethanolamine-N-[methoxy(polyethylene glycol)] (DSPE-PEG) (880120P, Sigma-Aldrich) in a molar ratio of 55:40:5. Using a 20-gauge needle, the lipid solution was rapidly injected into an equal volume of PBS under continuous rapid stirring at 72 °C. After 5 minutes, four volumes of PBS were added, and the solution was stirred for an additional 15 minutes at room temperature. The lipid solution for 70 kDa FTIC-dextran loaded liposome formation was rapidly injected into an equal volume of FITC-dextran solution, and the resulting liposomes were passed through a nanoporous membrane 7 times before use, with concentration determined by the Stewart assay.

2.3. MNV and F-MNV size characterization

Nanovesicle visualization was examined using transmission electron microscopy (TEM, Jem2100, JEOL, Tokyo, Japan) by staining the samples with 1% uranyl acetate for 30 seconds and dried for 1 hour on a Formva-carbon coated grid. The nanovesicle size distribution was analyzed through nanoparticle tracking analysis (NTA, Nanosight NS300, Malvern Panalytical, Malvern, UK). Nanovesicles were diluted in PBS in 1:10000 dilution and passed through microfluidic observatory camera settings in NTA device. Each flow was captured for 1 minute and repeated 3 times. Zeta-

potential of nanovesicles were analyzed by Zeta potential Analyzer (ELS-Z1000, Otsuka Electronics Ltd., Tokyo, Japan), with nanovesicles diluted in PBS in 1:20000 dilutions.

2.4. Flow cytometry

2.4.1. F-MNV fusogen identification

The expression of surface fusogens between immature MNV, MNV, and F-MNVs were analyzed with a flow cytometer (FACS Verse III, BD bioscience, Becton, NJ, USA).[15] 40 μg of nanovesicles were incubated with 1 μL of 4 μm diameter aldehyde/suface-latex beads (A37304, Invitrogen) in 1mL PBS. The solution was kept on a rocker overnight at RT. The reaction was stopped by incubation with glycine (110 mM, GR1021-100-00, BioSesang, Yongin, Republic of Korea) for 30 minutes. The suspension was then centrifuged at 14,000 × g for 30 minutes. The pellet was washed twice with 1 mL PBS with 0.5% FBS. After centrifugation, pellets were suspended in 100 uL PBS with 0.5% FBS with primary antibodies against E-cadherin (1:100, 3915, CellSignaling, Danvers, MA, USA), CD44 (1:100, NBP1-47386; Novus Biologicals, Centennial, CO, USA), and DC-STAMP (1:100, NBP1-79329, Novus Biologicals) and incubated at RT for 30 minutes. The suspension was centrifuged at 14,000 × g for 30 minutes and was washed twice with 1 mL PBS with 0.5% FBS. The pellets were suspended 100 uL PBS with 0.5% FBS with secondary antibodies against anti-mouse (1: 400, 115-095-003, Jackson Immuno Research), and anti-rabbit (1:500, 111-545-003, Jackson Immuno Research) and incubated at RT for 30 minutes. The suspension was washed twice and suspended in 400 uL of PBS with 0.5% FBS and were analyzed with flow cytometry.

2.4.2. Macrophage-EC coculture

To evaluate the targeting of vesicles to human umbilical vein endothelial cells (HUVEC) or macrophages, the coculture was detached and sorted by their biomarkers. Red fluorescent protein expressing HUVECs were sorted with red fluorescence, and macrophages were labeled with FTIC-conjugated CD11b (1:100, MA1-10081, Thermofisher) for 30 minutes in a 4 °C cold room, and then washed twice with PBS containing 2% FBS. The resulting cell mixture was centrifuged at 700 × g for 3 minutes and the pellet was suspended in PBS with 2% FBS for flow cytometry. FlowJo software (V10, BD Bioscience) was used for analysis. HUVEC and macrophages populations were divided based on their fluorescence tag and quantified the DiD-labeled vesicle uptake proportion of each population.

2.5. Macrophage targeted uptake assay

2.5.1. Macrophage monoculture

To measure uptake amount of MNV in macrophages and fusogenic macrophages, each cell was seeded (2.5×10^5 cells/well) onto a 24-well plate with glass-like polymer bottom (P24-1.5P, Cellvis, Ontario, Canada). MNVs were labeled with DiO (V22886, Thermo Fisher) and dispersed in complete DMEM medium, then treated to cells, incubated for 1 hour, and washed twice with PBS. For immunofluorescence staining, samples were fixed with 4 % PFA in PBS 30 minutes at RT and washed three times using PBS. For permeabilization, treated 0.2 % Triton X-100 and blocked with 5 % BSA in PBS. The cell cytoskeleton was stained with Rhodamine Phalloidin (1:1000, R415, Thermofisher) and counter stained with DAPI (R37606, Thermofisher). Confocal imaging was performed visualization and subjected to confocal imaging. DiO-NV imaging, and quantification of green fluorescence (DiO) between samples were analyzed with ImageJ.

2.5.2. Macrophage-EC coculture

For coculture analysis, HUVECs were cultured in 24-well culture plates, and 10 ng/mL TNF-α was added to the cells to induce inflammation 1 day before seeding macrophages at a 1:1 ratio with HUVECs for overnight. DiD labeled liposome (1 μmol/mL), MNV (25 μg/mL), and F-MNV (25 μg/mL) were treated to the coculture for 1 hour and washed twice with PBS. The coculture system was stained for immunofluorescence with primary antibody against vWF (1:200, ab6994, Abcam), anti-rabbit AlexaFluor488 secondary antibody (1:500, 111-545-003, Jackson Immuno Research), and DAPI. Confocal imaging was performed and analyzed using the ZEN software, and quantitative vesicle fluorescence (DiD) localized to macrophages for each group images was conducted using ImageJ (Fiji). Flow cytometry of the same coculture was analyzed by staining endothelial cells against vWF and macrophages against CD11b (1:200, MA-10080, ThermoFisher), and analysis using FlowJo software.

2.6. Macrophage fusion-mediated uptake assay

2.6.1. Non-fusion mediated uptake inhibition

For the non-fusion mediated uptake inhibition assay, all non-fusion mediated vesicle uptake mechanisms were inhibited: 20 μM cytochalasin D for actin (8273, Sigma-Aldrich), 25 μM nystatin for caveolin (N6261, Sigma), and 12.5 μM chlorpromazine hydrochloride for clathrin (C8138-5G, Sigma-Aldrich).[16] The concentrations were chosen based on liposome uptake inhibition which is known to be internalized by macrophages by actin, caveolin, and clathrin-mediated mechanisms. After 30 minute treatment of the inhibitors to macrophages, DiO-labeled liposome (1 μmol/mL), MNV (25 μg/mL), and F-MNV (25 μg/mL) were treated to macrophages seeded (2.5×10^5 cells/well) onto a 24-well plate with glass-like polymer bottom (P24-1.5P, Cellvis) overnight, followed by immunofluorescence staining with Rhodamine Phalloidin and DAPI. Confocal imaging and ImageJ

were used to quantify vesicle fluorescence (DiO) uptake of macrophages for each group.

2.6.2. Lysosome colocalization assay

For lysosome colocalization analysis we visualized the intracellular fate of particles loaded into vesicles. 70 kDa FITC-dextran were loaded in liposomes (1 μmol/mL) and MNVs (25 μg/mL) and treated to macrophages seeded the same way as the fusion assay for 1 hr. After PBS wash twice, cells were stained for immunofluorescence with PE-CD107a (1:100; Biolegend, 121612) and DAPI. Confocal imaging and ImageJ were used to quantify the colocalization of PE-labeled lysosome with FITC-dextran using the JACoP plugin for Pearson's coefficient. Z-stacks were taken with the same software to evaluate where the fluorescence lies within the cell, whether dextran was delivered to lysosomes or the cytosol.

2.7. Rabbit carotid artery plaque model

Rabbits (3 kg, male, New Zealand White) were purchased from Doo Yeol Biotech (Seoul, Republic of Korea) and acclimated to a large animal care facility for 1 week before use. Each rabbit was anesthetized through intramuscular injection of zoletil (10 mg/kg, ZoletilTM, Virbac Korea, Seoul, Republic of Korea), and anesthesia was sustained with endotracheal inhalation of isofluorane (2.2%, Hana Pharm, Gyeonggi, Republic of Korea). An incision was made at the anterior center of the neck to expose the carotid artery for dissection of the subcutaneous tissue and neck muscles. The bypass branches of the carotid artery were tied to prevent leakage artery blood using ST-B-1V 8 mm length single micro vessel clamp (00396, StarkMed, Artarmon, Australia), facilitating easier identification of the surgical location after harvesting the samples. Then, both the proximal and distal ends of the carotid artery were clamped using 6-0 black silk, and a line threaded through the 2 m inner diameter silicon tube was used to occlude the vessel. As a model of the right carotid artery of each rabbit was subjected to 2 mm incision and immediately ligated using 9-0 ethilon sutures. For confirmation of the leakage and blood flow, untied silicon tube and the neck soft-tissue was closed using a 4-0 vicryl suture, followed by skin closure using 4-0 ethilon suture. After the surgeries, the rabbits were closely monitored every day for 28 days. Pain management was achieved by administering meloxicam (0.5 mg/kg, Medica Korea, Seoul, Republic of Korea) orally once daily for the initial 7 days. To prevent infection, enrofloxacin (10 mg/kg, CTBio Inc., Hwaseong-si, Gyeonggi-do, Republic of Korea) was given orally during the first 7 days post-surgery. After 28 days, each rabbit was anesthetized with an intramuscular injection of zoletil (50 mg/kg) and xylazine (5 mg/kg), and the surgical ligation point of the neck carotid artery was opened. The samples were harvested after ligating the distal and proximal arteries with 6-0 black silk, and euthanasia was subsequently performed *via* intravenous injection of potassium chloride (20 mg/kg, Choongwae Pharma Corporation, Seoul, Republic of Korea). Arteries were imaged before and after incubation with 25 μg/mL of DiD-labeled F-MNV in PBS using the IVIS Spectrum (PerkinElmer, Waltham,

MA, USA) at a wavelength of 644/665 nm for DiD fluorescence localization.

2.8. Carotid angiography

Angiography was performed before harvesting samples using C-arm X-ray equipment (General Electric, NY, USA), by making an incision at the anterior center of the neck to expose the carotid artery. A hole was created in the proximal direction, at least 2 cm away from the incision point, using a flexible central venous catheter needle. Next, a 4-French catheter was positioned in the proximal hole, and a mixture of normal saline and contrast media (1:1 ratio, Scalnux, SANOCHEMIA, Austria) was injected through the catheter to capture images of the vessels.

2.9. Immunohistochemistry

Excised vascular tissues were fixed overnight at 4°C in 10% formalin prepared in PBS and washed three times with PBS. After fixation, samples were embedded in paraffin, sectioned at 4 μm thickness, and stained with hematoxylin and eosin (H&E) according to standard protocols. Images were captured using a Thunder microscope (Leica, Wetzlar, Germany). For immunofluorescence staining, tissue sections were deparaffinized and rehydrated through a graded series of xylene and ethanol solutions (100%, 95%, 80%, and 70% in deionized water). Antigen retrieval for MMP9 and CD68 detection was performed using high pH retrieval buffer (k800421-2, Agilent Dako, Santa Clara, CA, USA). To block endogenous peroxidase activity, slides were treated with 3% hydrogen peroxide (H2O2; H1009, Sigma Aldrich) for 10 minutes and then rinsed with tris-buffered saline (TBS; ML023-03, Welgene). Nonspecific binding was minimized by blocking with 5% bovine serum albumin (BSA) in PBS. Slides were then incubated overnight at 4°C with primary antibodies against MMP9 (1:100, Novus Biologicals, NBP2-13173) and CD68 (1:200, Novus Biologicals, NBP2-32831). The next day, after three PBS washes, sections were treated with Alexa Fluor 594-conjugated AffiniPure secondary antibodies (1:1000, Jackson ImmunoResearch) specific for the primary antibodies for 1 hour at room temperature. Cell nuclei were counterstained with DAPI, and specimens were visualized using a confocal microscope (LSM 780, Zeiss). Arterial elastin was detected by its natural autofluorescence at 488 nm. Quantitative image analysis was performed with ImageJ (Fiji).

2.10. qRT-PCR

Total RNA was extracted from carotid arteries with Trizol (Invitrogen) by incubation within the lumen for 3 minutes. Extracted RNA was measured for purity and quantity using a NanoDrop™

2000 Spectrophotometer. AccuPower® CycleScript RT Premix (Bioneer) was added to the RNA samples, and complementary DNA to the RNA was produced according to the manufacturer's instructions using the T-100 Thermal Cycler (Bio-Rad). qPCR was carried out with the resulting cDNA, primer set, and SYBR Green PCR mix on StepOne Plus Real Time PCR System (Applied Biosystems), then melting curves were analyzed. All the results were normalized to the amount of housekeeping gene glyceraldehyde 3-phosphate dehydrogenase (GAPDH). The values were calculated with the comparative Ct (2-ΔΔCt) method and further normalized to the negative control. The primer sequences used for the reaction are listed below in **Table 1**.

2.11. Statistical analysis

Statistical analysis was performed using GraphPad Prism software (GraphPad Software, San Diego, CA, USA). Two groups were compared with the two-tailed Student's t-test. Multiple group comparisons were made with one-way analysis of variance, with Tukey's post-hoc test for pair-wise comparisons. Statistical significance was calculated at a p-value of less than 0.05. The figures represent the p-values as *, **, and *** for $p < 0.05$, $p < 0.01$, and $p < 0.001$, respectively, with dashed lines indicating the groups being compared. Data were represented as the mean ± SEM, with units of measurements.

<Table 1> List of RT-PCR primers

	Primer sequence (5'-3')
TNF-α	Forward: CCGTCTCCTACCCGAACAAG
	Reverse: AAGGTCCAGGTACTCAGGCT
IL-1β	Forward: TGTCAGTCGTTGTGGCTCTG
	Reverse: TTGCAGAGGACGGGTTCTTC
IL-12	Forward: CCACAAAACCCCTCCCTTGA
	Reverse: AGGCATGGGGTCATCCTTCA
MMP-9	Forward: CGGAGACGGGTATCCTTTCG
	Reverse: CGGCGTTTCCAAAGTACGTG
E-cadherin	Forward: TCGCCTACGAAATCCTCAGC
	Reverse: TCTGCGGGTTGATCCTGAAC
CD44	Forward: TGCCTACCATGGCTCAGATG
	Reverse: ACGTGCCCTTCTATGAACCC
DC-STAMP	Forward: TGTCCTCCCGCTGAGTAAGA
	Reverse: CCAGAAAGACGGGACGACAA
GAPDH	Forward: GACCACTTCGGCATTGTGGA
	Reverse: ATGCCAGTGAGTTTCCCGTT

3. Results

3.1. Fusogenic macrophage differentiation by macrophage activation

To harvest a stable source of macrophage-derived nanovesicles (NVs), the C57BL/6 mice, 6 weeks old, were used to harvest the bone marrow cells from the femurs and tibias. Hematopoietic stem cells were cultured for six days with murine macrophage colony-stimulating factor (M-CSF, 100 ng/mL) to differentiate them into macrophages. The procedure for the production of fusogenic macrophages is depicted in the schematic **<Figure 1a>**.

After differentiation, the mature macrophages were then stimulated with interleukin-4 (IL-4, 100 ng/mL) for six additional days to induce the formation of multinucleated giant cells (MGCs). Immunofluorescence imaging **<Figure 1b>** showed progressive morphological changes with macrophage fusion. On day 3 after stimulation with IL-4, the macrophages were larger, with greater cytoplasmic area, and clustering typical of a fusogenic phenotype. Multinucleated cells were observed, suggesting peak fusogenic activity, likely caused by the upregulated expression of membrane-bound fusogens. On day 6, widespread cell fusion led to the formation of MGCs.

According to this temporal profile, the nanovesicles were isolated at two time intervals: i) from non-activated macrophages (day 0) for the isolation of baseline macrophage nanovesicles (MNVs), and ii) from day 2 after the stimulation with IL-4 for the preparation of fusogenic macrophage nanovesicles (F-MNV), which retains the fusogenic characteristics of the parent cell physiological state.

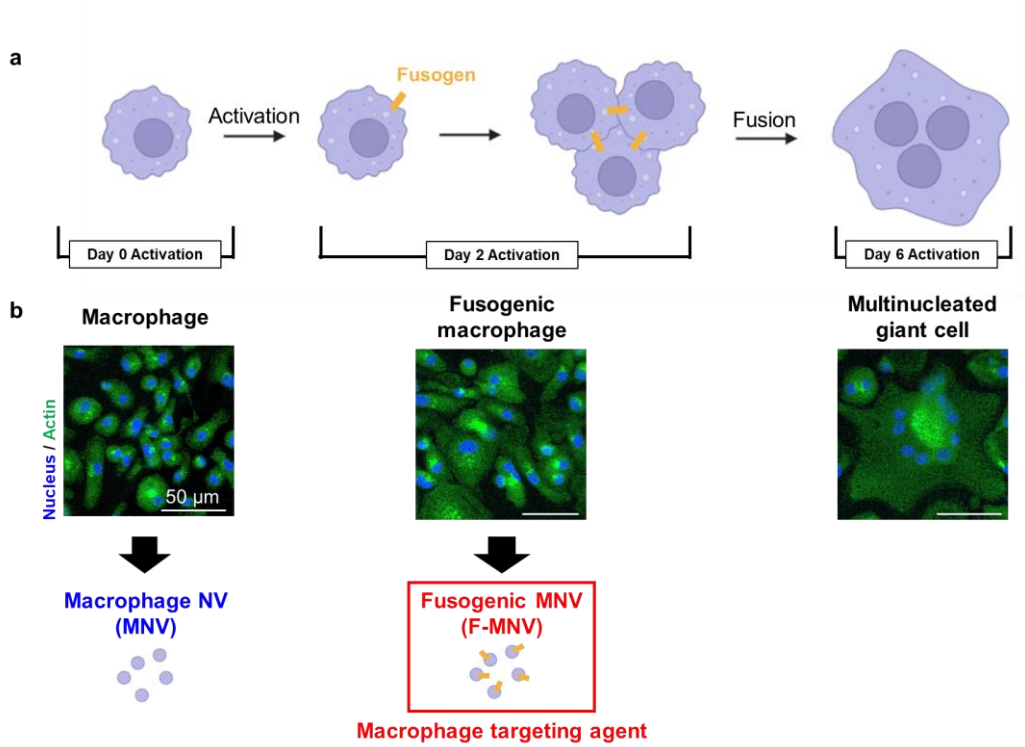

<Figure 1> Schematic representation of macrophage activation and fusion. a) Macrophages were activated with IL-4 (100 ng/mL) to acquire fusogenic properties, expressing fusogens on their surface by Day 2. These fusogenic macrophages subsequently fused to form multinucleated giant cells by Day 6. **b)** Immunocytochemistry images depict the activation timeline. Left: macrophages (Day 0) stained for nucleus (blue) and actin (green). Middle: fusogenic macrophages (Day 2) showing enhanced cell-cell interactions mediated by fusogens. Right: multinucleated giant cells (Day 6) formed through fusion of fusogenic macrophages. Scale bars: 50 μm. Nanovesicles extruded from macrophages and fusogenic macrophages are potential macrophage targeting agents. Abbreviations: MNV, macrophage-derived nanovesicles; F-MNV, fusogenic macrophage-derived nanovesicles.

3.2. Fusogenic macrophage-derived nanovesicle (F-MNV) extrusion and characterization

Obtaining nanovesicles of uniform size and stability is critical. Small variations in properties can impact safety and efficacy within circulation. To control the size and quality of F-MNVs, cells were passed through a 0.4 μm-pore polycarbonate membrane 7 times before usage **<Figure 2a>**. When macrophages pass through the pores, frictional force between the plasma membrane and the suface of the nanoporous membrane induces cell rupture into phospholipid bilayer fragments, followed by immediate self-assembly into nanospheres due to hydrophobic, hydrophilic interactions.[17]

Successful formation of nanovesicles was observed after extrusion **<Figure 2b-d>**. Nanovesicles were imaged with transmission election microscopy to verify their morphology **<Figure 2b>**. The macrophages were transformed into a 100 nm spherical shape with a fully enclosed phospholipid bilayer. Size analysis was further measured through nanoparticle tracking analysis. **<Figure 2c>**. Nanovesicles dispersed in PBS were introduced into a microfluidic optical microscope and a video was taken to capture the nanoparticle size range of the fluidic particles. Analyzed particles had a mean diameter of 99.6 nm, with the most distribution at 99.7 nm. The standard deviation was 5.6 nm, meaning the nanovesicle size were uniformly distributed around 100 nm size. Moreover, normalization to surface protein amounts quantified by the bicinchoninic acid (BCA) assay was used to estimate particle yield, revealing that approximately 10^7 particles are present per 1 μg of F-MNV.

Another key parameter for nanovesicles is their stability, which is analyzed through their zeta-potential. Cell-derived nanovesicles were artificially produced, often unstable relative to naturally secreted exosomes if not properly managed. F-MNV exhibits a zeta-potential of -42.51 mV **<Figure 2d>**. Zeta-potential is meaningful for nanovesicles because it indicates colloidal stability. Nanoparticle suspensions with a high absolute zeta-potential (> |30 mV|) are considered stable, meaning that they possess sufficient electrostatic repulsive force between each particle reducing aggregation.[18] Moreover, the negative charge is promising becuase negatively surface charge is advantageous for in vivo applicaitons due to their enhanced stability in biologcial fluids. Together, these results demonstrate that this extrusion method yields monodisperse, structurally intact, and highly stable F-MNVs.

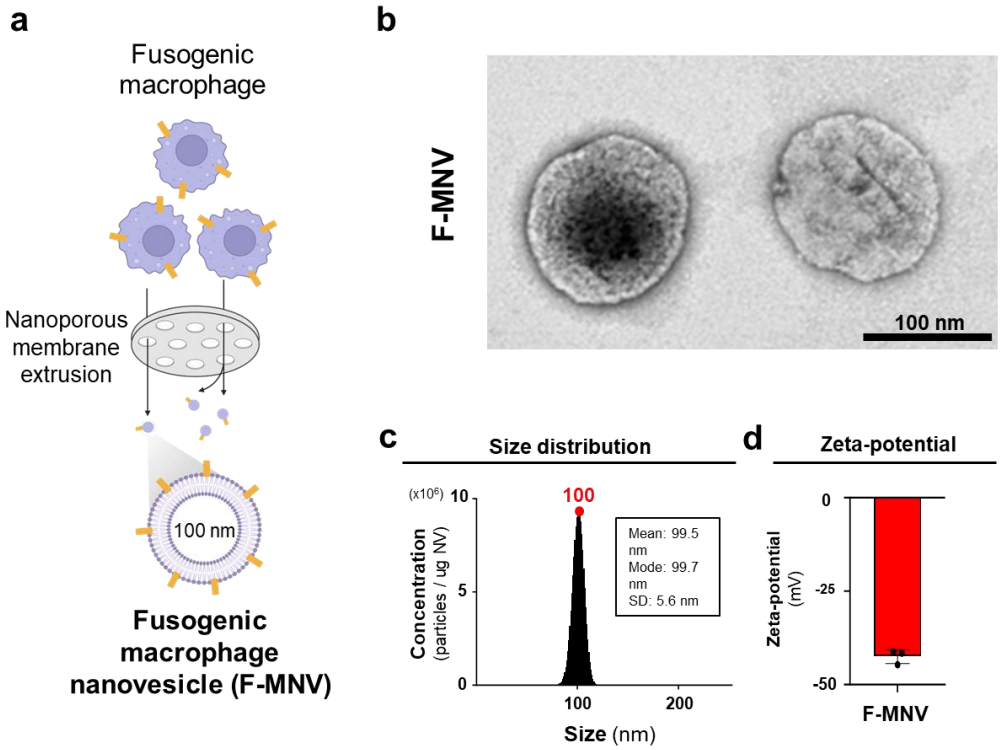

<Figure 2> Characterization of F-MNV. a) Schematic representation of F-MNV production via mechanical extrusion. Fusogenic macrophages were processed through a 0.4 μm-pore polycarbonate membrane to extrude nanovesicles with an average size of 100 nm. **b)** Transmission electron microscopy (TEM) image of F-MNVs, confirming their spherical morphology and uniform structure. Scale bar: 100 nm. **c)** Nanoparticle tracking analysis (NTA) showing the size distribution of F-MNVs with a mean size of 99.5 nm, mode of 99.7 nm, and standard deviation (SD) of 5.6 nm. **d)** Zeta-potential analysis demonstrating the stability of F-MNVs, with a negative surface charge indicative of colloidal stability.

3.3. Bead-assisted flow cytometric analysis of surface-displayed fusogenic markers on F-MNVs

Fusogenic macrophages transiently display specific surface proteins that promote cell-cell fusion preceding the formation of multinucleated giant cells (MGCs). Nanovesicles purified from such macrophages (F-MNVs), from the peak fusogenic phase, would likely retain membrane-bound fusogenic proteins that mark the cell of origin. Such fusogen-bearing nanovesicles would potentially function as endogenously armed macrophage-targeting entities with the support of endogenous recognition and adhesion molecules.

Owing to their small size (~100 nm), the nanovesicles cannot be detected directly by conventional flow cytometry. To avoid this, the F-MNVs were tagged with 4 μm polystyrene beads, and the surface markers were detectable and quantifiable by bead-assisted flow cytometric analysis <**Figure 3**>. This technique also enabled the comparison of the expression of the fusogenic markers in the three macrophage stages: monocyte-like immature macrophages, mature macrophages, and fusogenic macrophages.

Three widely characterized fusogenic proteins were chosen for examination: E-cadherin, CD44, and dendritic cell-specific transmembrane protein (DC-STAMP).[19-21] Both E-cadherin and CD44 are adhesion molecules that are involved in macrophage-macrophage interaction and clustering, which are prerequisites for subsequent fusion. DC-STAMP, a transmembrane protein specifically upregulated in fusion-competent macrophages, is involved in the essential function of cell-cell fusion through its role in the mediation of recognition and signaling among fusogenic cells.

Bead-assisted flow cytometry revealed specific expression profiles for the subpopulations of macrophage-derived nanovesicles. F-MNVs were distinguished by the significantly greater expression of all three fusogenic markers compared with MNVs from non-fusogenic or immature macrophages. DC-STAMP expression was exclusively observed in F-MNVs, confirming its utility as a specific marker for the activated, fusion-competent macrophage phenotype. The absence of DC-STAMP in earlier stages of macrophage development further confirms its utility as a selective indicator of fusogenic conversion. These findings show that F-MNVs retain signature membrane-bound fusogenic features of the cells from which they were derived, for the benefit of their potential use toward targeting macrophage populations and enabling fusion-dependent cell interactions in downstream uses.

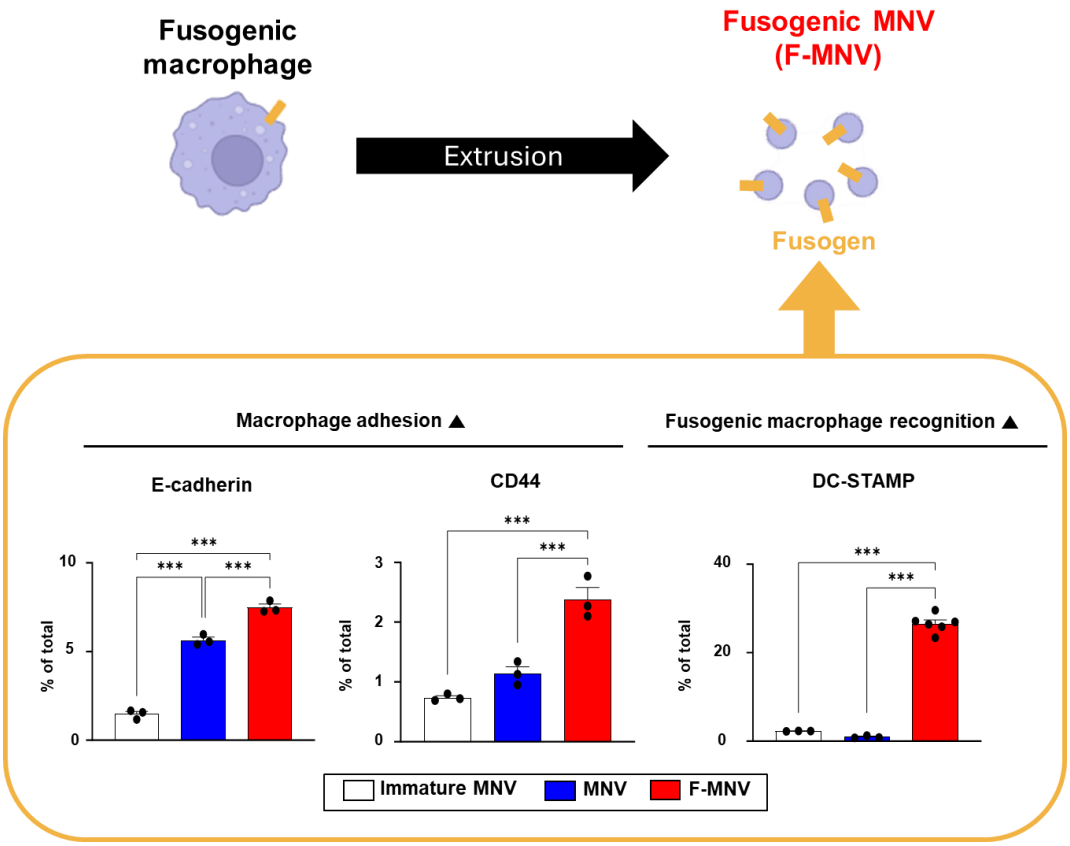

<Figure 3> Identification of surface fusogenic proteins on F-MNVs. Flow cytometry analysis identifying key fusogens of F-MNVs compared to immature macrophage-derived nanovesicles (Immature MNV) and macrophage-derived nanovesicles (MNV). E-cadherin and CD44 were associated with macrophage adhesion, while DC-STAMP was identified as a marker for fusogenic macrophage recognition. Data are presented as mean ± SD. Statistical significance: *p < 0.05, **p < 0.01, ***p < 0.001 between indicated groups.

3.4. Fusogen-mediated enhancement of nanovesicle internalization by macrophages *in vitro*

The purpose of this study was to determine whether fusogenic modification enhances the uptake of nanovesicle (NV) by macrophages. To this end, in vitro uptake assays were conducted with DiO-labeled NVs and confocal fluorescence microscopy.

The results indicated that the fusogenic macrophages exhibited enhanced uptake of the NVs. <**Figure 4a**> illustrates that macrophages and fusogenic macrophages were incubated with DiO-labeled macrophage-derived NVs (MNVs) for one hour. High intracellular accumulation of the NV (green) in the fusogenic macrophages, relative to the low intracellular accumulation in the normal macrophages, was observed with confocal microscopy. To confirm intracellular localization of the NV, the actin cytoskeleton and nuclei were stained with phalloidin (red) and DAPI (blue), respectively. The quantitation of the NV signal area per cell revealed considerably higher NV uptake in the fusogenic macrophages, with approximately 3-fold higher internalization relative to the unmodified macrophages (****$p < 0.0001$).

Furthermore, fusogenic MNVs (F-MNVs) showed greatly enhanced macrophage uptake efficiency. To ascertain whether the increase in this process is mediated by fusogenic modification of the NVs themselves, macrophages were incubated with MNVs or with fusogenic MNVs (F-MNVs) under the same conditions **<Figure 4b>**. Confocal microscopy revealed a significant increase in internalized green fluorescence in the cells incubated with F-MNVs compared with MNVs. Counting the number of NVs per cell also confirmed this result, with approximately a 5-fold increase with F-MNVs compared with MNVs (***$p < 0.001$).

Together, these findings emphasize the point that fusogenic modification has the ability to greatly increase the uptake of NV by macrophages, both when used to modify target cells and when the fusogenic modification has been incorporated into the NVs themselves.

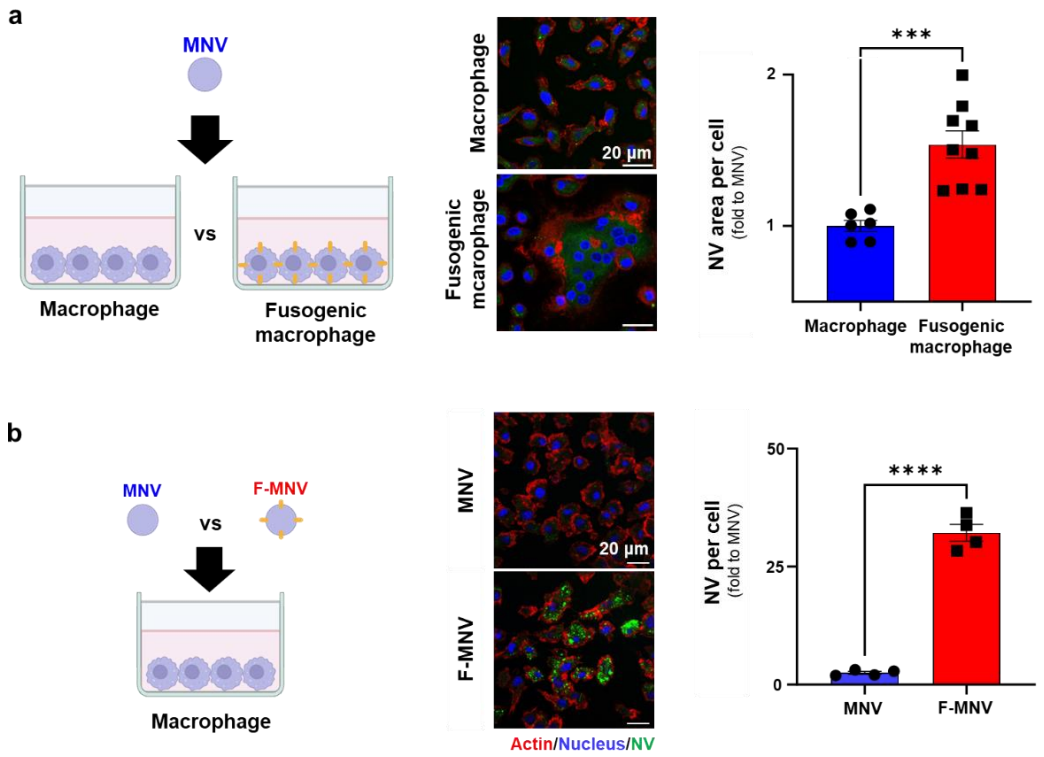

<Figure 4> ***in vitro*** **analysis of enhanced NV uptake by macrophages mediated by fusogens.**
a) Comparative analysis of NV uptake by macrophages and fusogenic macrophages. DiO(green)-labeled macrophage-derived nanovesicles (MNVs, 25 μg/mL) were incubated with macrophages and fusogenic macrophages for 1 hour. Confocal microscopy images show intracellular NV localization, with nuclei (blue) and actin (red) staining. Quantitative analysis reveals significantly higher NV uptake by fusogenic macrophages compared to regular macrophages. Scale bars: 20 μm. **b)** Enhanced uptake of fusogenic macrophage-derived nanovesicles (F-MNVs) compared to MNVs in macrophages. DiO-labeled MNVs and F-MNVs (25 μg/mL) were treated to macrophages for 1 hour, followed by confocal imaging to assess NV internalization. Quantitative analysis shows a substantial increase in NV uptake with F-MNVs compared to MNVs. Data are presented as mean ± SD. Statistical significance: *$p < 0.05$, **$p < 0.01$, ***$p < 0.001$, ****$p < 0.0001$ between indicated groups.

3.5. Enhanced uptake of fusogenic macrophage-derived nanovesicles (F-MNVs) by macrophages in an artery-mimetic endothelial-macrophage coculture

To determine the macrophage-targeting ability of fusogenic nanovesicles in a more physiologically relevant context, we used the *in vitro* artery-mimetic endothelial cell–macrophage coculture model.

F-MNVs show preferential macrophage uptake in endothelial coculture. Immunofluorescence microscopy revealed dramatic differences in the internalization of vesicles between treatment groups **<Figure 5a>**. DiD-labeled liposomes, macrophage-derived nanovesicles (MNVs), or fusogenic macrophage-derived nanovesicles (F-MNVs) were incubated with the coculture system for 1 hour. The endothelial cells were stained with green vWF, and nuclei were stained with blue. Widespread F-MNV internalization throughout the culture was observed under low magnification. Under higher magnifications, the clear enrichment of F-MNVs in macrophages (vWF-) was obvious by the intense red accumulation of the vesicles around the nucleus (white arrowheads). MNVs were moderately internalized, and liposomes were minimally internalized by macrophages. Quantitative image analysis confirmed that macrophages that were treated with F-MNVs accumulated much more vesicles than macrophages that were treated with MNVs or liposomes (****$p < 0.0001$).

Flow cytometric analysis confirms selective F-MNV internalization by macrophages. To better quantify cell-type-selective vesicle internalization, endothelial cells (vWF+) and macrophages (CD11b+) were separated from the coculture by flow cytometry and DiD-positive internalization of the vesicles assessed **<Figure 5b>**. From macrophages, treatment with F-MNV yielded the highest number of vesicle-positive cells (57%), followed by MNVs (45%), and liposomes (10%). Less than 2% of endothelial cells in all treatments confirmed preferential targeting of macrophages. Macrophage quantitation of the internalization of the vesicles confirmed imaging findings, with F-MNVs performing significantly better than MNVs (**$p < 0.01$) and liposomes (***$p < 0.001$).

Together, the data indicate that fusogenic engineering of macrophage-derived nanovesicles greatly enhances targeting and internalization by macrophages, even in the context of the complex coculture model of endothelial cells and macrophages that mimic the vascular environment.

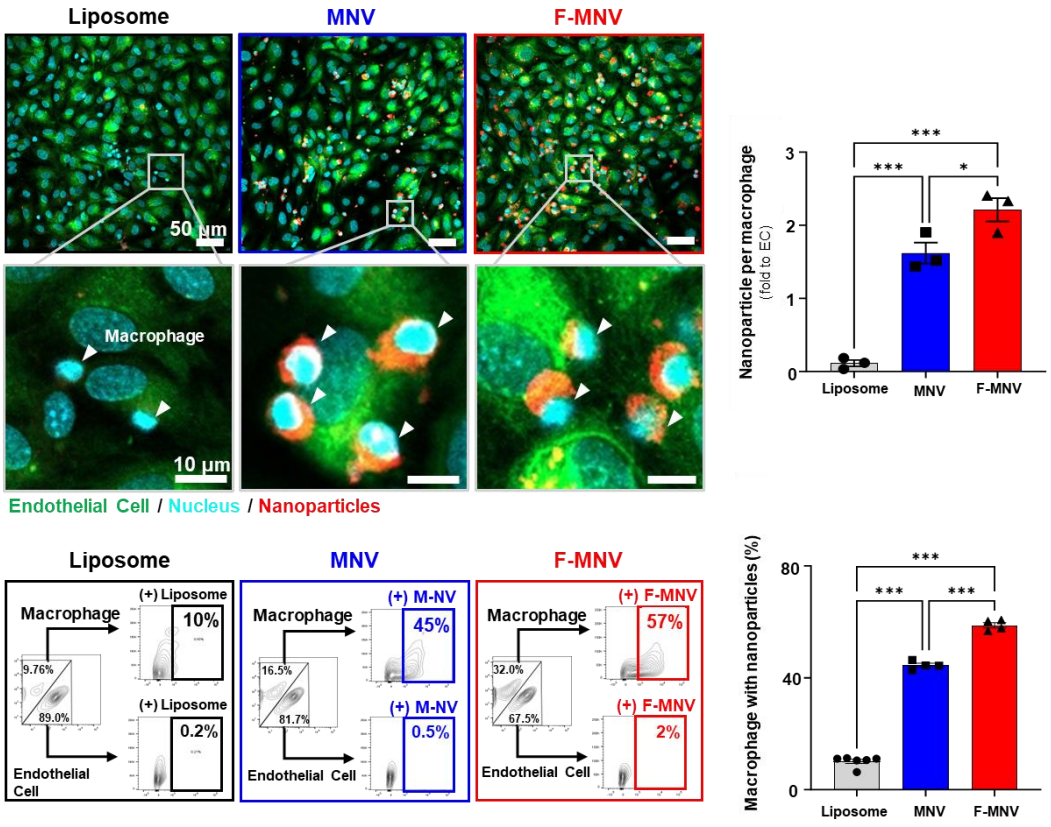

<Figure 5> ***in vitro*** **macrophage-targeted uptake in artery-mimetic endothelial cell-macrophage coculture. a)** Confocal microscopy analysis of macrophage-specific NV internalization in a coculture of endothelial cells and macrophages. DiD(red)-labeled liposomes (1 μmol/mL), macrophage-derived nanovesicles (MNV, 25 μg/mL), and fusogenic macrophage-derived nanovesicles (F-MNV, 25 μg/mL) were treated for 1 hour. Cells were stained for nuclei (blue) and endothelial cell marker vWF (green). Images indicate preferential uptake of F-MNVs by macrophages compared to liposomes and MNVs. Quantitative analysis confirms F-MNVs exhibit the highest uptake efficacy. Scale bars: 50 μm (top), 10 μm (bottom). **b)** Flow cytometry-based sorting of endothelial cell (vWF) and macrophage (CD11b) populations with internalized DiD-vesicles from the coculture reveals significantly enhanced F-MNV uptake by macrophages relative to liposomes and MNVs. Data are presented as mean ± SD. Statistical significance: *p < 0.05, **p < 0.01, ***p < 0.001 between indicated groups.

3.6. Fusion-based cargo delivery by F-MNVs avoids lysosomal degradation in macrophages

To confirm that fusogenic macrophage-derived nanovesicles (F-MNVs) transported cargo by membrane fusion and not by endocytic pathways, we used a series of mechanistic uptake and lysosomal colocalization experiments in macrophages.

Internalization of F-MNV is not heavily inhibited by endocytic pathway blockage. To ascertain the classical endocytosis dependence of F-MNV internalization, macrophages were pre-treated with inhibitors for clathrin-mediated endocytosis (chlorpromazine), for caveolin-mediated endocytosis (nystatin), or for actin-dependent uptake (cytochalasin D), and then incubated with DiO-labeled vesicles overnight **<Figure 6>**. Confocal microscopy revealed liposomes and MNVs exhibited significantly diminished green intensity per cell after inhibition, indicative of diminished uptake. F-MNV uptake, though, remained relatively constant under all conditions of inhibition, as indicated by constant green intensity of the signal. Quantitative analysis verified endocytic inhibitors significantly inhibited liposome and MNV uptake (***$p < 0.001$, ****$p < 0.0001$), but F-MNV uptake was inhibited to a lesser degree, suggesting the presence of another, fusion-mediated entry process independent of the classical endocytic pathways.

F-MNVs exhibit low colocalization with lysosomes, implying endosome bypass. To further validate fusion-mediated cargo delivery, we also examined colocalization of the vesicle contents with lysosomes by dual-labeling. Macrophages were treated with liposomes or F-MNVs containing FITC-dextran for 1 hour and stained for nuclei (blue) and lysosomes (red, LAMP-1) **<Figure 7a>**. Under confocal microscopy, there were strong yellow signal (green-red overlap) in dextran-liposome-treated cells, indicating trafficking of the vesicular cargo to lysosomes via endocytic uptake. In contrast, F-MNV-treated cells had largely nonoverlapping green and red signals with less yellow puncta (white arrows), indicating minimal lysosomal localization. Quantitative analysis by Pearson's colocalization coefficient also verified significantly less colocalization of F-MNV cargo with lysosomes as compared to liposomes (***$p < 0.001$). Moreover, from a distance profile of the cells in **<Figure 7b>**, liposome treated cells exhibit a same fluorescence in locations of lysosomes, meaning that the cargo is delivered to lysosomes, susceptible to degradation. **<Figure 7c>** also verifies that the cargo of F-MNVs is successfully internalized into the cell cytosol, of which cargo signal can be seen in the cell cytosol rather than simple adherence to the membrane.

These data support that F-MNVs utilize a fusion-based entry mechanism into macrophages, enabling efficient cytoplasmic delivery of cargo while evading lysosomal degradation.

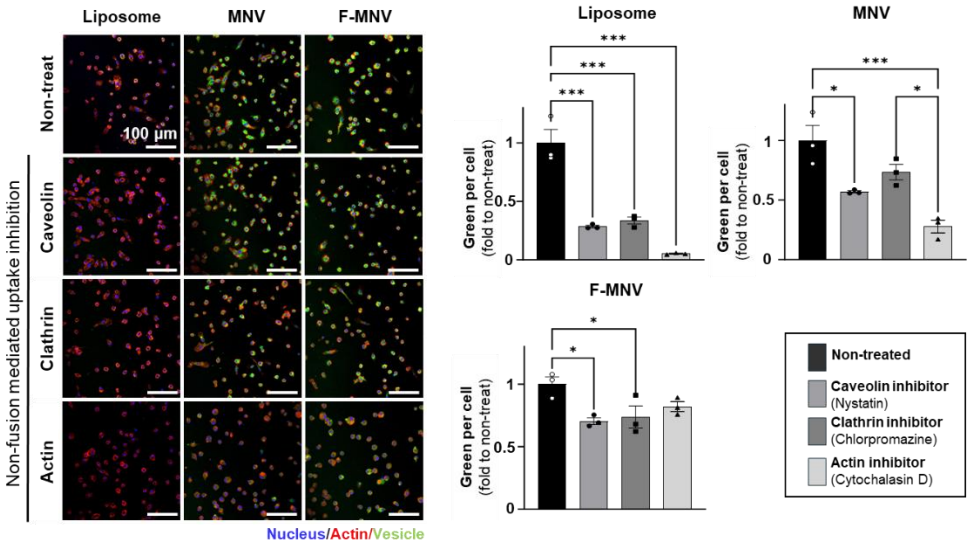

<Figure 6> ***in vitro*** **fusion-mediated uptake assay of F-MNV by non-fusion inhibition.** a) Macrophages were treated with inhibitors targeting non-fusion mediated uptake mechanisms (caveolin, clathrin, and actin-mediated pathways). Cells were exposed overnight to DiO (green)-labeled liposomes (1 μmol/mL), macrophage-derived nanovesicles (MNV, 25 μg/mL), and fusogenic macrophage-derived nanovesicles (F-MNV, 25 μg/mL). Staining was performed for nuclei (blue) and actin (red). Quantitative analysis indicates that F-MNV uptake was least affected by the inhibition of non-fusion pathways. Scale bars: 100 μm. Data are presented as mean ± SD. Statistical significance is indicated as follows: *p < 0.05, **p < 0.01, ***p < 0.001 between indicated groups.

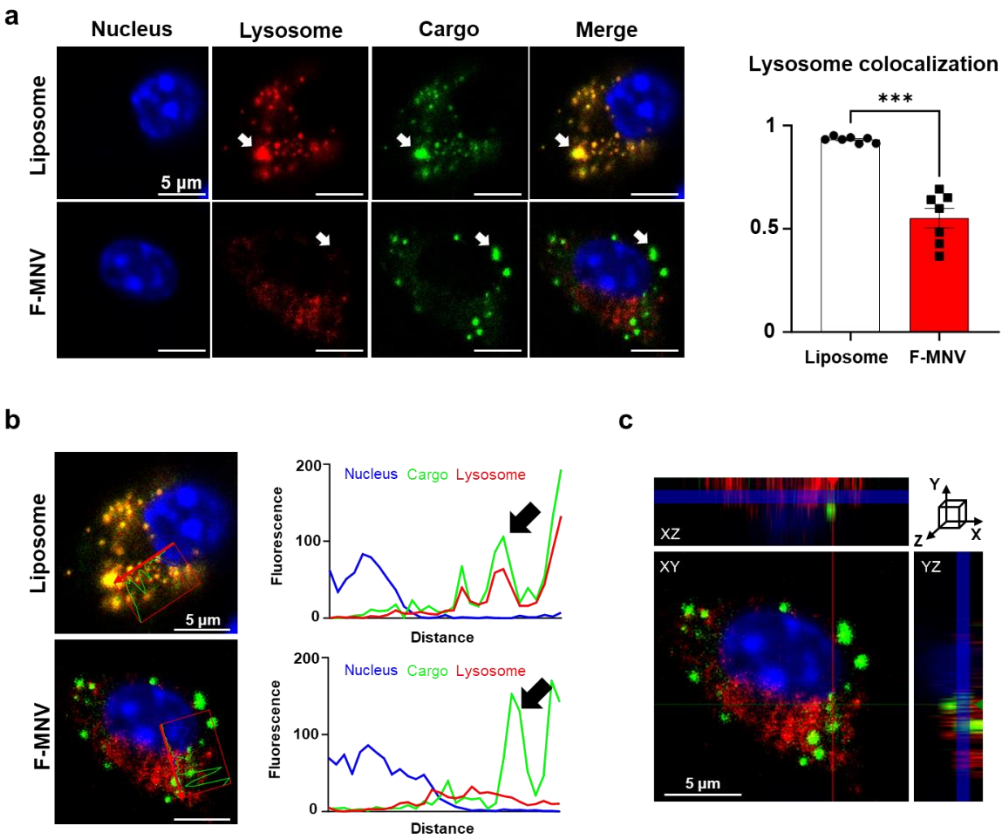

<Figure 7> ***in vitro*** **fusion-mediated uptake assay of F-MNV by lysosome colocalization analysis.** A lysosome colocalization study was conducted using FITC-dextran (70kDa) loaded liposomes and F-MNV cargo delivery, analyzed via confocal imaging. Macrophages were treated with 1 μmol/mL dextran-liposome and 25 μg/mL dextran-F-MNVs for 1 hour, followed by staining for nuclei (blue) and lysosomes (red, LAMP-1). **a)** Colocalization with lysosomes was quantified using Pearson's coefficient. Scale bars: 5 μm. **b)** Fluorescence profiles starting from the nucleus (blue) to the FITC-dextran (green) and lysosome (red) to the end of the cell show that liposome delivered cells show direct correlation of cargo fluorescence density with lysosome density, while F-MNV shows high signals in areas of low lysosome signals. Scale bars: 5 μm. **c)** Orthogonal view of the cell verifies intercellular uptake of F-MNVs. Scale bar: 5 μm. Data are presented as mean ± SD. Statistical significance is indicated as follows: *p < 0.05, **p < 0.01, ***p < 0.001 between indicated groups.

3.7. Rabbit carotid injury-induced plaque formation and F-MNV targeting efficiency imaging

To determine the targeting capability of fusogenic macrophage-derived nanovesicles (F-MNVs) in vivo, we employed the rabbit carotid artery plaque model. This model offers a clinically relevant and physiologically appropriate system to investigate targeted nanovesicle delivery in the context of vascular injury and the early stages of atherosclerotic disease. As depicted in **<Figure 8a>**, the model was established by inducing focal endothelial injury with needle puncture followed by carotid artery ligation, followed by the development of localized plaque over time. Through Week 4 after injury, visual examination revealed lesion-associated narrowing of the vessel, confirmed by angiographic imaging with intraluminal contrast injection. This method reproducibly induced vascular remodeling with atherosclerotic lesions, simulating the pathology of human plaques.

A rabbit model is particularly ideal for this study due to its well-characterized ability to undergo reproducible changes in atherosclerosis, including macrophage accumulation and fibrous plaques in the aorta and coronary arteries, with striking similarity to human atherogenesis. Rabbits also possess a more developed immune system compared to rodents, permitting more realistic modeling of the process of inflammation of atherosclerosis, including macrophage recruitment, foam cell formation, and cytokine signaling dynamics.

To ascertain the targeting ability of F-MNVs, DiD-labeled F-MNVs (25 μg/mL) were injected directly into the lumen of the arteries and incubated for three minutes, followed by PBS flush before imaging **<Figure 8b>**. Within injured arteries, intense fluorescent signals for DiD-labeled vesicles were observed exactly where the luminal narrowing took place. These regions, demarcated by yellow arrowheads, also showed retention of contrast and morphological changes characteristic of the development of plaque. In contrast, uninjured arteries did not exhibit any significant accumulation of F-MNVs, with low background signals. Fluoroscopic imaging, IVIS scans, and photographical recording collectively confirmed that F-MNVs accumulated preferentially in injured vascular regions. The findings verify the validity of F-MNVs as precision nanocarriers for targeted delivery or for the molecular imaging of cardiovascular disease.

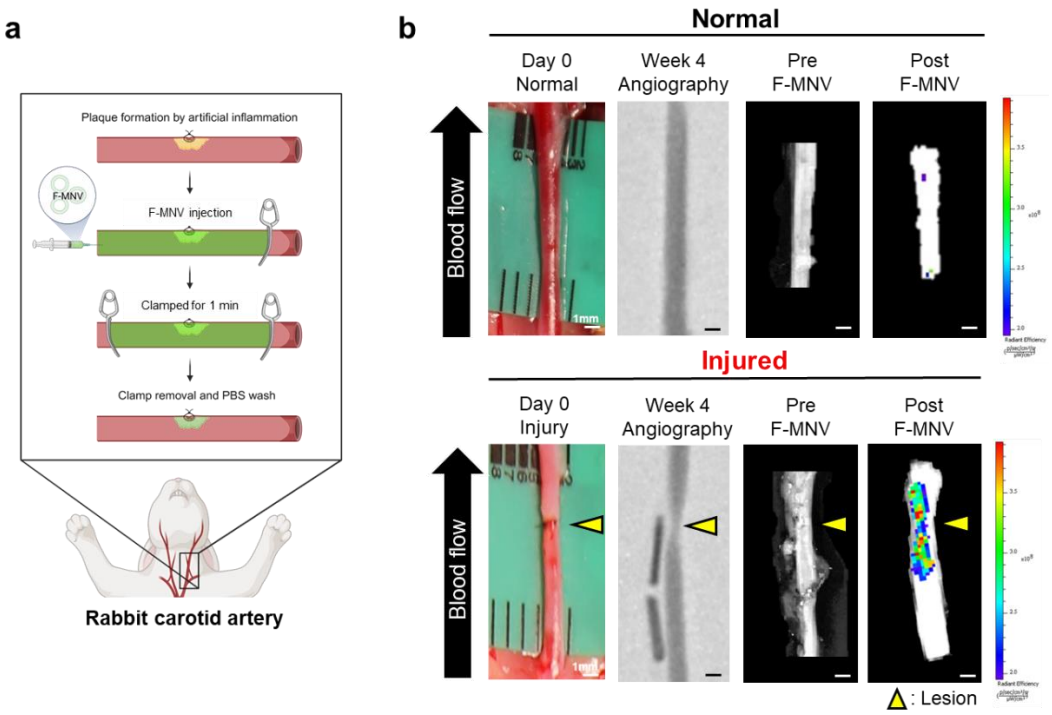

<Figure 8> ***in vivo*** **rabbit carotid artery plaque model formation. a)** Schematic illustrating the model creation process involving needle puncture and subsequent suturing to induce plaque formation. Fluorescent F-MNVs were introduced to the vessel after clamping and washed after 1 minute incubation with PBS. **b)** Photographs of arteries were taken on Day 0 of the surgical procedure. The narrowed lesion areas were identified by injecting a contrast agent into the artery lumen on Week 4. Arteries were harvested and imaged using IVIS before and after injection of DiD-labeled F-MNV (25 μg/mL) into the lumen. F-MNV was incubated for 3 minutes, followed by a PBS wash prior to IVIS imaging. Scale bars: 1 mm.

3.8. F-MNVs localize to macrophage-rich regions of vulnerable carotid artery plaques

To better characterize the *in vivo* localization of fusogenic macrophage-derived nanovesicles (F-MNVs) within arteries with plaques, the areas of intense signal observed by IVIS imaging were dissected out and were analyzed by histological and immunofluorescence examination for colocalization with the primary cellular and structural elements of vulnerable atherosclerotic lesions.

As seen in **<Figure 9a>**, H&E staining of resected carotid artery segments exhibited striking differences in lesion-bearing and normal arteries. The normal arteries exhibited an intact trilaminar structure, with absence of any indication of plaque formation. Lesioned arteries, but not the normal arteries, exhibited significant neointimal thickening, with extensive necrotic core (NC) and thin fibrous cap of approximately 20 μm width—indicative of a vulnerable plaque phenotype. The neointima (N) was thickened considerably and displaced the normal vascular geometry, suggesting advanced lesion development and increased risk of rupture.

To determine whether F-MNVs were preferentially targeted to regions of inflammation within these plaques, the same regions were interrogated by immunofluorescent staining for elastin (yellow), nuclei (blue), and markers of inflammation. **<Figure 9b>** shows strong expression of the pro-inflammatory markers matrix metalloproteinase-9 (MMP-9) and macrophage marker CD68 in the neointimal space. These pro-inflammatory signatures colocalized with the regions of elastin-degraded, macrophage-rich areas where strong F-MNV signal had already been detected. The elastin fibers delineating the medial layer (M) were disrupted adjacent to areas of dense macrophage accumulation, characteristic of extracellular matrix remodeling and weakening typical of rupture-prone plaques.

These findings confirm that F-MNVs preferentially accumulate in macrophage-rich and MMP-9-positive regions of the neointima, particularly in structurally vulnerable regions of the plaque. This topographical correlation proves the usefulness of F-MNVs for targeting the inflammatory microenvironments of unstable atherosclerotic lesions, confirming their therapeutic as well as diagnostic potential in advanced vascular disease.

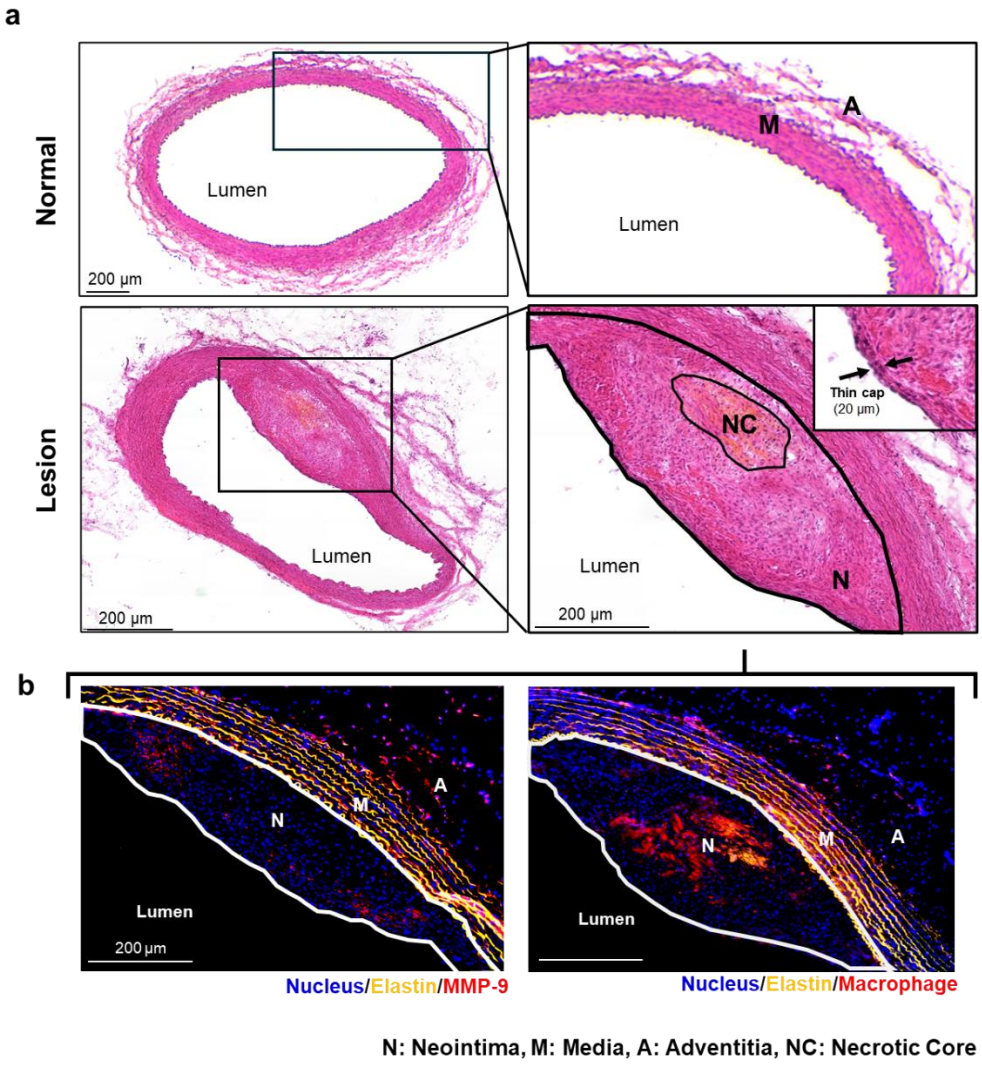

<Figure 9> F-MNV localizes to macrophage-rich vulnerable plaque areas of the carotid artery model. High signal F-MNV areas were excised for histological analysis. **a)** H&E staining of normal and lesion sections reveals the neointimal area, characterized by a rupture-prone thin fibrotic cap and necrotic core. **b)** Immunohistological staining of the same area shows a high presence of inflammatory macrophages (CD68, MMP-9). Scale bars: 200 μm.

3.9. Upregulation of inflammatory and fusogenic markers in F-MNV-targeted plaques

To molecularly verify the selective targeting of fusogenic macrophage-derived nanovesicles (F-MNVs) to inflammatory atherosclerotic plaques, quantitative reverse transcription PCR (qRT-PCR) analysis of RNA extracted from injured and uninjured normal rabbit carotid arteries was conducted. This was to investigate the expression of the major inflammatory and fusogenic markers in regions with proven F-MNV accumulation.

Injured arteries exhibited significantly enhanced mRNA expression of pro-inflammatory cytokines and atherosclerosis progression-associated matrix remodeling enzymes. Tumor necrosis factor-alpha (TNF-α), interleukin-1 beta (IL-1β), and interleukin-12 (IL-12) were considerably upregulated in injured arteries when compared to controls, indicating the active inflammatory microenvironment. Moreover, the extracellular matrix-degrading, plaque vulnerability-associated matrix metalloproteinase-9 (MMP-9) showed considerable overexpression in injured arteries. These results are consistent with the histological and immunostaining results of Figure 8, where the accumulation of macrophages and the occurrence of MMP-9 were noted within the neointimal area **<Figure 10a>**.

In addition to the inflammatory markers, we also compared the expression of membrane fusion and vesicle uptake-related genes **<Figure 10b>**. Pathological arteries showed the upregulated expression of the cell–cell fusion and macrophage multinucleation-related proteins E-cadherin, CD44, and dendritic cell-specific transmembrane protein (DC-STAMP). The upregulated expression of the fusogenic markers in the F-MNV-targeted regions suggests that the cell environment in the targeted regions is conducive for the fusion-based mechanisms of uptake, which supports the observed increase in F-MNV localization to pathological vascular tissue.

Collectively, these qRT-PCR findings offer molecular confirmation that F-MNVs selectively target the inflamed and fusion-competent regions of the damaged vasculature, substantiating the promise of F-MNVs as a precision delivery platform for cardiovascular inflammatory disorders.

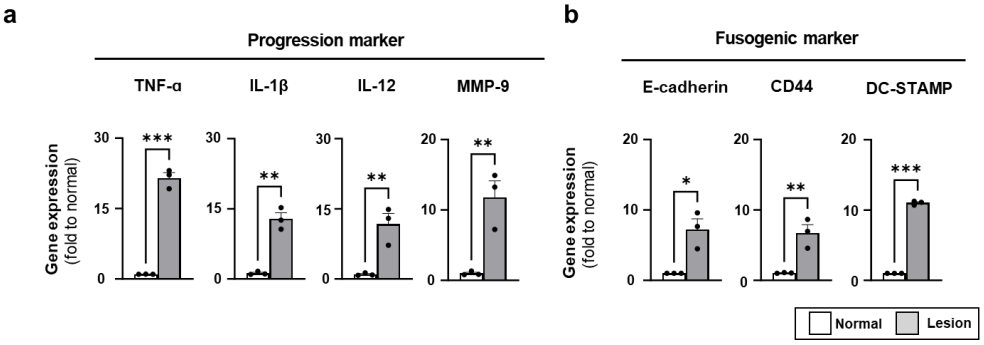

<Figure 10> qRT-PCR analysis confirms selective targeting of inflammatory atherosclerotic plaques by F-MNVs. a) Increased expression of plaque progression markers (TNF-α, IL-1β, IL-12, MMP-9) and **b)** fusogenic markers (E-cadherin, CD44, DC-STAMP) were observed in injured arteries. Data are presented as mean ± SD. Statistical significance is indicated as follows: *p < 0.05, **p < 0.01, ***p < 0.001, ****p < 0.0001 between indicated groups.

4. Discussions

The present research offers all-inclusive framework on designing, characterization and validating fusogenic macrophage-derived nanovesicles (F-MNVs), in the first place as a new class of inflammation-specific nanocarrier, alluding mainly to atherosclerosis-related vascular disease. With a variety of *in vitro* and *in vivo* experiments, we prove that F-MNVs engineered to retain fusogenic membrane proteins from activated macrophages acquire better cellular uptake, strong specificity towards targeting macrophage-rich lesions, and efficient deliveries of its cargo into cytoplasmic compartments, avoiding endo-lysosomal degradation. These findings back up the potential use of such precision delivery systems for diagnosing and chemical control purposes in diseases attributable to inflammatory processes.

Our approach is that during chronic inflammation macrophages have a fusogenic phenotype, which results in the up-regulation of E-cadherin and CD44, typical markers of adhesion molecules, as well as the transmembrane fusogen DC-STAMP. F-MNVs were obtained with surface-displayed fusogens confirmed through bead-assisted flow cytometry **<Figure 3>** by harvesting macrophages at their peak fusogenic state. This endogenous protein signature differentiates F-MNVs from common nanovesicles derived from macrophages (MNVs) and provides a biological basis for their improved targeting to select macrophages.

Structural and biophysical characterization of F-MNVs showed good characteristics for application *in vivo*. Vesicles of about 100 nm, with narrow polydispersity and high colloidal stability (zeta potential -42 mV) **<Figure 2>** were generated by extrusion through nanoporous membranes. Thus, pharmacokinetics can be kept consistently, minimize agglomeration and will result in greater circulation stability. Moreover, TEM imaging confirms the forming enclosed spherical nanostructures that have a native-exosome-like morphology, but customizable surface content.

A major finding of this study is that F-MNVs, as compared to both MNVs and regular liposomes, were associated markedly increased rates of cellular uptake in macrophages **<Figures 4, 5>**. This was both in monocultures and in a coculture model of endothelial cells and macrophages that recapitulates the vascular interface. Confocal microscopy and quantitative fluorescence analysis confirmed that exposure of macrophages to F-MNVs resulted in significantly increased vesicle internalization. Further evidence for macrophage-selective uptake of F-MNVs was acquired using flow cytometry, with a significant number of endothelial cells remaining untargeted—thus showing the selectivity of this nanovesicle system for immune cell populations.

Mechanistic dissection of the uptake pathways revealed that F-MNV internalization is largely independent of traditional endocytic routes **<Figure 6>**. Pharmacological inhibition of clathrin, caveolin, or actin-dependent pathways significantly reduced uptake of liposomes and MNVs, but had minimal impact on F-MNV internalization. This supports a fusion-based mechanism, whereby vesicles directly merge with the plasma membrane to release their contents. Furthermore, lysosomal colocalization assays demonstrated that F-MNV cargo avoids endosomal trafficking and lysosomal degradation **<Figure 7>**, an advantageous feature for efficient cytoplasmic delivery of

labile or bioactive cargo. To investigate targeting efficacy in vivo, we utilized a surgically induced rabbit carotid artery plaque model that mimics features of human atherosclerosis, including plaque formation, macrophage infiltration, and fibrous cap thinning **<Figure 8>**. F-MNVs selectively accumulated at sites of vascular injury and plaque development, as visualized by IVIS and confirmed by histological analysis **<Figures 8 and 9>**. H&E and immunostaining revealed F-MNV localization to macrophage-rich areas of the neointima, particularly within regions expressing high levels of MMP-9 and CD68, and characterized by structural markers of plaque vulnerability (i.e., thin fibrous caps and necrotic cores). These spatial correlations reinforce the biological targeting capacity of F-MNVs for inflamed, high-risk atherosclerotic lesions. Finally, qRT-PCR analysis of excised arteries revealed strong upregulation of pro-inflammatory cytokines (TNF-α, IL-1β, IL-12) and matrix-degrading enzymes (MMP-9) in injured arteries, along with elevated expression of fusogenic markers E-cadherin, CD44, and DC-STAMP **<Figure 10>**. These molecular signatures align with the histological observations and further support that F-MNVs home to and accumulate in inflammatory, fusion-competent vascular environments. Collectively, these findings establish fusogenic nanovesicles as a powerful bioinspired platform for macrophage-targeted delivery. Unlike synthetic nanoparticles, F-MNVs inherit both the surface complexity and membrane behavior of their parent cells, allowing for biologically programmed targeting and membrane fusion. Their ability to bypass endocytic degradation, combined with their specificity for macrophage-rich inflammatory lesions, makes them uniquely suited for addressing chronic inflammatory diseases such as atherosclerosis, tuberculosis, or autoimmune disorders. Future studies may extend this approach by incorporating therapeutic cargo, surface modifications, or imaging agents for translational application in diagnostics and targeted nanomedicine.

5. Conclusion

In this study, we developed and validated a novel fusogenic macrophage-derived nanovesicle (F-MNV) platform for targeted delivery to macrophage-rich, inflammatory atherosclerotic lesions. By leveraging the natural process of macrophage fusion, F-MNVs were generated from macrophages at their peak fusogenic phase, resulting in nanovesicles enriched with membrane-bound fusogens such as E-cadherin, CD44, and DC-STAMP. These features conferred selective binding and fusion-mediated uptake in target macrophages, distinguishing F-MNVs from conventional nanocarriers that rely on receptor-mediated endocytosis.

F-MNVs possess favorable biophysical properties, including monodisperse size (~100 nm), stable zeta potential, and preserved bilayer morphology. Functional analyses showed that F-MNVs exhibit significantly enhanced uptake by macrophages, both in monoculture and in endothelial-macrophage coculture systems. Notably, this uptake was minimally affected by classical endocytosis inhibitors, and confocal microscopy confirmed their cytosolic delivery bypassing lysosomal degradation—highlighting the role of direct membrane fusion in their mechanism of entry.

In a rabbit carotid artery injury model that recapitulates key aspects of human atherosclerosis, F-MNVs selectively accumulated at lesion sites characterized by macrophage infiltration, MMP-9 expression, and fibrous cap thinning. Histological and molecular analyses confirmed that F-MNV localization correlated with markers of plaque vulnerability and inflammation. These findings establish F-MNVs as effective, biologically derived nanocarriers for targeting inflammatory vascular disease.

Hence, this work introduces F-MNVs as a robust and versatile platform for cell-targeted nanomedicine, offering unique advantages in selectivity, uptake efficiency, and biological compatibility. The integration of fusogenic cues into nanovesicle engineering opens new opportunities for precise drug delivery and imaging applications in inflammatory disorders, particularly in cardiovascular disease. Future studies may build upon this foundation to deliver therapeutic agents or gene-editing tools directly to diseased tissue sites with enhanced specificity and minimal off-target effects.

References

1. Hetherington I, Totary-Jain H. Anti-atherosclerotic therapies: milestones, challenges, and emerging innovations. Molecular Therapy 2022;30:3106-17.
2. Jebari-Benslaiman S, Galicia-García U, Larrea-Sebal A, Olaetxea JR, Alloza I, Vandenbroeck K, et al. Pathophysiology of atherosclerosis. International journal of molecular sciences 2022;23:3346.
3. Kim JB, Park K, Ryu J, Lee JJ, Lee MW, Cho HS, et al. Intravascular optical imaging of high-risk plaques in vivo by targeting macrophage mannose receptors. Scientific reports 2016;6:22608.
4. Helming L, Gordon S. Molecular mediators of macrophage fusion. Trends in cell biology 2009;19:514-22.
5. Xiao Z, Li Y, Xiong L, Liao J, Gao Y, Luo Y, et al. Recent advances in anti-atherosclerosis and potential therapeutic targets for nanomaterial-derived drug formulations. Advanced Science 2023;10:2302918.
6. Tewabe A, Abate A, Tamrie M, Seyfu A, Abdela Siraj E. Targeted drug delivery—from magic bullet to nanomedicine: principles, challenges, and future perspectives. Journal of Multidisciplinary Healthcare 2021:1711-24.
7. Qiu C, Xia F, Zhang J, Shi Q, Meng Y, Wang C, et al. Advanced strategies for overcoming endosomal/lysosomal barrier in nanodrug delivery. Research 2023;6:0148.
8. Lee SY, Cheng JX. Clearance of nanoparticles during circulation. Pharmaceutical Sciences Encyclopedia: Drug Discovery, Development, and Manufacturing 2010:1-32.
9. Pei D, Buyanova M. Overcoming endosomal entrapment in drug delivery. Bioconjugate chemistry 2018;30:273-83.
10. Li W, Gonzalez KM, Chung J, Kim M, Lu J. Surface-modified nanotherapeutics targeting atherosclerosis. Biomaterials science 2022;10:5459-71.
11. Pang AS-R, Dinesh T, Pang NY-L, Dinesh V, Pang KY-L, Yong CL, et al. Nanoparticles as drug delivery systems for the targeted treatment of atherosclerosis. Molecules 2024;29:2873.
12. Tao Y, Lan X, Zhang Y, Fu C, Liu L, Cao F, et al. Biomimetic nanomedicines for precise atherosclerosis theranostics. Acta Pharmaceutica Sinica B 2023;13:4442-60.
13. Song R, Bafit M, Tullett KM, Tan PS, Lahoud MH, O'Keeffe M, et al. A Simple and Rapid Protocol for the Isolation of Murine Bone Marrow Suitable for the Differentiation of Dendritic Cells. Methods and Protocols 2024;7:20.
14. Pons M, Foradada M, Estelrich J. Liposomes obtained by the ethanol injection method. International journal of pharmaceutics 1993;95:51-6.
15. Suárez H, Gámez-Valero A, Reyes R, López-Martín S, Rodríguez MJ, Carrascosa JL, et al. A bead-assisted flow cytometry method for the semi-quantitative analysis of Extracellular Vesicles. Scientific reports 2017;7:11271.
16. Yu SE, Kim J, Kim DH, Baek S, Park S, Chung S, et al. Time-Controlled Dual Targeting

to Program Systemic and Intercellular Transfer of Therapeutic Effects. Advanced Functional Materials 2025:2418560.

17. Jo W, Kim J, Yoon J, Jeong D, Cho S, Jeong H, et al. Large-scale generation of cell-derived nanovesicles. Nanoscale 2014;6:12056-64.
18. Pochapski DJ, Carvalho dos Santos C, Leite GW, Pulcinelli SH, Santilli CV. Zeta potential and colloidal stability predictions for inorganic nanoparticle dispersions: Effects of experimental conditions and electrokinetic models on the interpretation of results. Langmuir 2021;37:13379-89.
19. Yagi M, Miyamoto T, Sawatani Y, Iwamoto K, Hosogane N, Fujita N, et al. DC-STAMP is essential for cell–cell fusion in osteoclasts and foreign body giant cells. The Journal of experimental medicine 2005;202:345-51.
20. Sterling H, Saginario C, Vignery A. CD44 occupancy prevents macrophage multinucleation. The Journal of cell biology 1998;143:837-47.
21. Van den Bossche J, Bogaert P, Van Hengel J, Guérin CJ, Berx G, Movahedi K, et al. Alternatively activated macrophages engage in homotypic and heterotypic interactions through IL-4 and polyamine-induced E-cadherin/catenin complexes. Blood, The Journal of the American Society of Hematology 2009;114:4664-74.

Abstract in Korean

대식세포 유래 융합 나노베지클을 통한 동맥경화성 플라크 진단

대식세포는 특정 자극 하에 서로 융합하여 다핵 거대세포로 형성될 수 있는 고유한 능력을 가지고 있다. 이 과정에서 대식세포는 융합성이 증가하고, 동종 융합을 촉진하는 특정 융합 매개 표면 단백질을 발현하게 된다. 세포 유래 소포체인 나노베지클은 세포 생리학의 특정 시점에서 세포막을 이용하여 생산될 수 있으며, 이 베지클들은 세포의 특정 생리학적 상태를 반영하게 된다. 본 연구에서는 새로운 대식세포 표적 약물 전달 시스템으로 융합성 대식세포 유래 나노소포(F-MNV)를 제안한다. F-MNV는 융합 매개체를 유지한 상태로 존재하여, 자연적으로 대식세포를 표적화할 수 있다. 이러한 F-MNV는 다양한 세포 집단 중에서도 대식세포에 선택적으로 흡수되는 특징을 가지고 있다. 또한, 기존의 나노입자 섭취 방식과 달리, F-MNV는 대식세포막과 직접 융합하여 세포질로 직접 약물을 전달할 수 있으며, 내포 소기관의 함정 효과(endosomal entrapment) 및 리소좀 분해(lysosomal degradation)를 우회할 수 있다. 토끼 동맥경화 모델에서 F-MNV는 대식세포가 풍부한 플라크를 효과적으로 표적화하여, 염증성 질환에서 정밀하고 생물학적으로 유래된 약물 전달 플랫폼으로서의 가능성을 입증하였다.

핵심되는 말 : 세포 유래 나노베지클, 대식세포 융합, 약물 전달 시스템, 동맥경화